ASSESSMENT OF PELLET INJECTION FOR NET

PART I:

Penetration depth calculations for single pellets on the basis of available ablation models

PART II:

Pellet sizes and velocities required for central fuelling based on available ablation models: feasibility considerations

L.L.Lengyel

IPP 1/231 September 1984

MAX-PLANCK-INSTITUT FÜR PLASMAPHYSIK

8046 GARCHING BEI MÜNCHEN

MAX-PLANCK-INSTITUT FÜR PLASMAPHYSIK

GARCHING BEI MÜNCHEN

ASSESSMENT OF PELLET INJECTION FOR NET

PART I:
Penetration depth calculations for single pellets on the basis of available ablation models

PART II:
Pellet sizes and velocities required for central fuelling based on available ablation models: feasibility considerations

L.L.Lengyel

IPP 1/231 September 1984

Die nachstehende Arbeit wurde im Rahmen des Vertrages zwischen dem Max-Planck-Institut für Plasmaphysik und der Europäischen Atomgemeinschaft über die Zusammenarbeit auf dem Gebiete der Plasmaphysik durchgeführt.

IPP 1/231 L. L. Lengyel

ASSESSMENT OF PELLET INJECTION FOR NET

Part I:
Penetration depth calculations for single pellets on the basis of ablation models available.

Part II:
Pellet sizes and velocities required for central fuelling based on ablation models available: feasibility considerations.

Abstract

In Part I results of penetration depth calculations applied to single pellets under thermonuclear plasma conditions are described. Calculations were performed for different pellet size and velocity combinations. Data corresponding to the neutral gas shielding ablation model and a magnetic shielding approximation are compared.

Part II (see page 11) is concerned with the pellet sizes and pellet velocities required for central fuelling. If only neutral gas shielding takes place, central fuelling with realistic pellet velocities is not possible. The presence of magnetic shielding may reduce the velocity requirements to technically feasible values. The study of the ablation physics and the development of comprehensive ablation models thus appear to be of primary importance.

Introduction

Pellet injection is considered as a potential candidate for fusion reactor fuelling that supplements, if not replaces, gas puffing /1/. In fact, pellet injection yields penetration depths and mass deposition profiles not accessible to gas puffing. Besides being a practical method of bringing fresh fuel into the inner plasma regions, pellet injection may possess a number of additional advantages: (i) it may open up a way of generating favourable temperature and density profiles, thus improving energy confinement in tokamaks; (ii) it may prove to be a method of extending the density limits observed in tokamaks; (iii) the flux and energy of cx neutrals leaving the plasma may be affected by building up high-density low-temperature plasma layers at pre-selected plasma depths; (iv) it may allow fast density ramp-up and ignition under thermonuclear plasma conditions.

Recent tokamak experiments have demonstrated the beneficial effects of pellet injection: a notable short-time density increase over the anticipated density limit has been observed in PDX /2/, and a substantial improvement of the energy confinement time has been obtained with the help of pellets in ALCATOR-C /3/. In view of the developments in the field of pellet injection, it has been decided to assess the applicability of pellet injection to large-scale fusion devices such as NET /4/. In the first parts of the present study, the exsisting ablation models are used for estimating the pellet sizes and velocities that would be required for affecting the plasma parameters in the inner region of NET (central fuelling). The uncertainties inherent in these calculations are discussed in later parts of this report series (see Part III and IV).

Numerical Modelling

A pellet injected into a magnetically confined hot plasma is subject to bombardment by species present in the recipient medium. As a result of the energy transfer to the pellet (surface or volume heating, depending on the penetration depth, i.e. the energy, of the incident particles) the material vaporizes, expands, and interacts with the recipient plasma. As a result of pellet-

plasma interaction, the local and global plasma characteristics are changed during the pellet ablation, which affects the ablation rate itself. Hence a self-consistent treatment of the process requires the coupling of an analytical or numerical pellet ablation model to a transport code that calculates the propagation of the temperature and density perturbations caused by the pellet in the background plasma.

Although the physical process considered is essentially three-dimensional (while the pellet is injected into the plasma across the magnetic field lines, the ablatant fills the confinement vessel by expanding in the poloidal and toroidal directions along the field lines and, at the same time, diffuses in the radial direction across the flux surfaces), the transport processes are considered in a one-dimensional approximation. If the ablated and ionized particles expand along the field lines with the thermal velocity of the plasma particles, the corresponding time scale is much shorter than the radial transport time (not considering anomalous transport and charge exchange effects /5/), and also shorter than the ablation time. It may thus be assumed that the ablated substance instantaneously fills the toroidal volume elements (toroidal annuli) and radial diffusion (classical or empirical) is the only transport process that should be considered in detail.

As is shown in Part III (see also /11/), owing to the "funnelling" of the ablatant in magnetic flux tubes, the time required for building-up a quasi-steady shielding layer around the pellet is comparable with the residence time of the pellet in the flux tube. Hence the assumption of instantaneous equilibration along the magnetic field lines may not always be valid. Nevertheless, for the time being we shall remain by this assumption.

In most calculations that follow, the neutral gas shielding ablation model /6/ is used in combination with the BALDUR 1D tokamak transport code /7/. In part of the calculations the reduction of the ablation rate due to magnetic shielding /8/ is taken into account. The merits and shortcomings of these ablation models

and approximations are discussed elsewhere (see Part III).

Recipient Plasma (input data for BALDUR)

The parameters of the recipient plasma where chosen in accordance with INTOR specifications (R = 5.2 m, a = 1.62 m, b/a = 1.6, B_Z = 5.5 tesla, I = 6.4 MA). A scrape-off version of BALDUR was used that allowed the particles diffusing to the scrape-off layer to be pumped off.

The discharge was built up within the first 5 s of the total discharge time (15 s) by means of gas puffing (D_2/T_2: 50 % to 50 %) and NB injection (D_2 beams with a total beam current of 0.634 kA, E_{max} = 175 keV; beam current fractions with 1, 1/2, and 1/3 of the max. beam energy of 0,42 0,38, and 0,2, respectively) to an average density and average temperature of $\langle n \rangle \simeq 1.5 \times 10^{20} m^{-3}$ and $\langle T \rangle \simeq 10$ to 12 keV. In the absence of pellets, the density was maintained at this level by gas-puffing, while the temperature and the maximum value of beta were regulated by a "soft-beta-limit" built into the code (the thermal conductivity of the electrons was increased exponentially with increasing β_{pol}: $\chi_e \propto \chi_{eo} \exp[\text{const.} \langle \beta_{pol} \rangle^2]$. In this way the maximum value of the toroidal β was limited to $\beta_{tor} \simeq 5$ % and the alpha-power produced to $P_\alpha \simeq 130$ MW.

A recycling coefficient of 0.9 was used, i.e. 90 % of the thermal plasma particles reaching the well were returned to the plasma as neutrals with an energy of 3 eV. The energetic cx neutrals lost were not included in the number of recycled particles: they were replaced by means of gas-puffing. In these runs, the recycled particles were fed to the plasma at a fictitious limiter radius, which, owing to deeper penetration, assured flat density profiles without the use of empirical inward drift terms. (Density profiles obtained without this limiter option may peak at the plasma edge.)

All ions entering the scrape-off layer were pumped off (divertor modelling) without any replacement. The parallel flow Mach numbers were assumed to be 0.02 both for helium and for the hydrogen isotopes. The connection length for the parallel flow was taken to be 81.7 m.

With regard to the dominating transport processes the following assumptions were made (r_{scr} denotes the inner radius of the scrape-off layer):

$$\begin{Bmatrix} D_{D,T} \\ D_{He} \\ \chi_e \end{Bmatrix} = \begin{Bmatrix} 0.2 \\ 0.2 \\ 1.0 \end{Bmatrix} \times 5 \times 10^{17}\, n_e\,(cm^{-3})^{-1} \qquad r < r_{scr}$$

$$\begin{Bmatrix} D_{D,T} \\ D_{He} \\ \chi_e \end{Bmatrix} = \begin{Bmatrix} 1.0 \\ 1.0 \\ 1.5 \end{Bmatrix} \times 10^{4} \qquad r > r_{scr}$$

The ion thermal conductivity χ_i was set equal to 3 times the simplified neoclassical value. In the case of helium, an inward drift term was also activated.

The alpha particle heating model included particle thermalization where the particle is deposited with allowance for first orbit losses.

Corona equilibrium was assumed while calculating radiative losses. Helium was considered as the only impurity present. Under these conditions, the total radiated power was approx. 12 MW during the steady-state discharge phase.

Some characteristics of the reference discharge are reproduced in Figs. 1 to 4. The radial temperature and density distributions are shown in Fig. 1 for the time t = 9.25 s (helium density peaking at the center and denoted by a dotted line is magnified tenfold). The time variations of the temperatures, electron densities (helium density multiplied by 10) and beta values are shown in Figs. 2,3 and 4, respectively. It should be noted that it was not intended to produce scenario simulations by means of these runs. Consideration was restricted to penetration depth investigations in a given discharge.

Two pellets were injected into this reference discharge after the plasma profiles became stabilized, viz. at ~9 s (D_2 pellet) and ~10 s (T_2 pellet) (in the case of a pellet velocity of 8000 m/s the tritium pellet was injected at t ≃ 11 s).

Pellet Data

The number densities of condensed deuterium and tritium at T ≃ 10 °K are $n_{D_2} \simeq 3.05 \times 10^{28}$ m^{-3} and $n_{T_2} \simeq 3.23 \times 10^{28}$ m^{-3}, respectively /9/. In this series of runs, pellets of radii 0.2 cm to 0.5 cm and velocities 2000 m/s to 8000 m/s were injected into the recipient plasma. The number of atoms in the pellets and the corresponding increase of the average density in INTOR (plasma volume ~ 207.81 m^3) are shown in Fig. 5 as functions of the pellet radius.

Note that, because of one-dimensionality, BALDUR neglects vertical plasma elongation and works with an effective radius value: $r_{eff} = (r_a \cdot r_b)^{1/2}$. Hence if pellets are injected into the torus in the meridional plane, the velocity required for a certain penetration depth (assuming constant plasma parameters) is reduced by a factor $(b/a)^{1/2} \simeq 1.26$ compared with the values given in our calculations (or, for a fixed pellet velocity, the calculated penetration depths may be increased by approximately this factor).

As can be seen, a pellet with an approx. $r_p \simeq 0.55$ cm radius would double the mean density in INTOR (~ 1.5×10^{20} m^{-3}). Note that for refuelling purposes a 10 to 20 % density increase per pellet seems reasonable. A 10 % average density increase corresponds to a pellet radius of $r_p \simeq 0.25$ cm.

Results of Calculations

(a) Neutral gas shielding ablation model

Figure 6 shows the radial density and temperature distributions in the recipient plasma before pellet injection (reference case for the first pellet). Figures 7 to 9 show the corresponding distributions after pellet injection (D_2 pellets) for an injection velocity of 4000 m/s and three pellet sizes: r_p = 0.2, 0.3, and

0.4 cm, respectively. Obviously, the larger the pellet, the larger is the penetration depth and/or the resulting density (and temperature) perturbation. (In the density distributions, the total electron density and the deuterium ion density are given by the upper and lower solid lines, respectively, while the tritium ion density is represented by the flat dotted line). As can be seen, for r_p = 0.4 cm the deuteron density peaks at r ≃ 105 cm, while the tritium ion density remains unchanged. Figure 10 corresponds to the same discharge as Fig. 9 and shows the distributions after the second (T_2) pellet has been injected (t = 10 s, the tritium ion density peaks at r ≃ 100 cm but the D^+ density profile is still hollow: it has not yet recovered from the D_2 pellet injection). The effect of the pellet velocity on the penetration depth and density profile can be seen from Figs. 11, 8, and 12, which corresponds to r_p = const = 0.3 cm and v_p = 2000, 4000, and 8000 m/s, respectively. Note that for this pellet size even the highest velocity tested is not sufficient for affecting the central plasma.

The results of penetration depth calculations are summarized in Fig. 13, where the penetration depths are given as functions of the pellet radii (both for D_2 and T_2 pellets) and the pellet velocities. Note that increasing the pellet velocity from 2000 m/s to 8000 m/s results in a rather moderate gain in penetration depth: only about 40 % at $r_p \simeq 0.5$ cm. This is due to the centrally peaked plasma temperature profile: the deeper the pellet penetrates, the hotter is the plasma it reaches. The ablation rate increases as approx. the 1.6 power of the electron temperature (neutral gas shielding ablation model /6/). The maximum temperatures "seen" by the injected pellets are plotted in Fig. 14 as functions of the pellet size and pellet velocity both for D_2 and T_2 pellets. At sufficiently large pellet sizes (deeper penetration) a T_2 pellet injected after a D_2 pellet (time delay: 1 or 2 s) "sees" a plasma cooled by the preceding pellet (deep penetration is associated with smaller flux tube volumes and larger adiabatic cooling effect). The temperatures

resulting from adiabatic cooling at the ablation front are also shown in this figure (only for D_2 pellets; see the three curves at the bottom of the plot). For example, a D_2 pellet with a 0.5 cm radius injected at 8000 m/s penetrates the plasma up to a layer of $T_e \simeq 19.8$ keV and cools down the plasma locally to $T_e \simeq 7.2$ keV. Owing to thermal conduction and alpha particle heating the temperature rapidly recovers. Nevertheless, a T_2 pellet injected 2 s later only sees a max. temperature of $T_e \simeq 17$ keV, although it penetrates almost 10 cm deeper than the D_2 pellet did.

A light scattering of the computed adiabatic temperature values (not shown in this figure) was observed: it is probably due to scattering in the diagnostic (print and plot) times and the approximate definition of the ablation front (defined approximately by maximum penetration depth).

(b) Magnetic shielding approximation

It has been observed in ablation experiments (see Part III of this report series and Ref. /10/) that at elevated temperatures the ablation rate is about an order of magnitude less than that predicted by the neutral shielding ablation model. Also the results of one-dimensional calculations in which the magnetic "funnelling" of the ionized pellet substance was taken into account showed approximately an order-of-magnitude reduction of the ablation rate (see Fig. 3 of Part III and Ref. /11/).

Reference /8/ presents a zero-dimensional model based on a set of conservation equations in which the convection of the magnetic field by the expending pellet-plasma and its re-diffusion into the ionized substance have been taken into account by calculating the corresponding magnetic Reynolds number and the associated reduction of the energy flux affecting the pellet ("magnetic diffusion model"). The ablation rates obtained in this approximation for a certain plasma electron density and a fixed pellet radius can be related to the respective plasma electron temperatures by means of a power law:

$$\dot{N}_2/\dot{N}_1 \approx (T_{e_2}/T_{e_1})^{0.43} .$$

We recell that the neutral gas shielding model implies a dependence of the form

$$\dot{N}_{n.g.s.} \propto r_p^{4/3} n_e^{1/3} T_e^{1.64}$$

(subscript n.g.s. denotes neutral gas shielding).

Let us now assume that the same r_p and n_e dependences apply in the presence of a magnetic field as in the neutral gas shielding model but the temperature dependence is close, at sufficiently high temperatures, to the 0.43 power law, i.e. the ablation rate is expressible as

$$\dot{N}_{m.s.} \propto r_p^{4/3} n_e^{1/3} T_e^{0.43}.$$

For the sake of simplicity, in a series of calculations it was assumed that

$$\dot{N} = \left(\frac{1.2}{T_e \text{ (keV)}}\right) \dot{N}_{n.g.s.} ,$$

i.e. the ablation rate calculated by the n.g.s. model was increased in the low-temperature region (in accordance with the results of /8/) and reduced proportionally to T_e^{-1} in the temperature region exceeding 1.2 keV. This is a rather crude approximation, but it does bear a resemblance to the experimental observations and to the results of the one-dimensional calculations mentioned.

The recipient plasma used in these transport calculations is a marginally ignited INTOR discharge with a central temperature of 19.6 keV before the moment of pellet injection (compared with 26 keV in the previous calculations).

The results of calculations are summarized in Table 1, in which the penetration depths and the maximum densities and temperatures

"seen" by the injected D_2 and T_2 pellets with a 0.3 cm radius are given for three pellet velocities both for the neutral gas and the magnetic shielding approximations used. (Time delay between a D_2 and T_2 pellet: 1 s.) As can be seen from the tabulated values, within the framework of the approximation used, magnetic shielding could substantially increase the penetration depths (approximately double them at sufficiently high velocities).

Table 1: Pellet penetration depths in an INTOR discharge and the max. temperatures and densities "seen" by the first (D_2) pellet. Pellet radius: 0.3 cm. Time delay between the two pellets: 1 s.

v (m/s)	l_{D_2} (cm)	l_{T_2} (cm)	T_e (ke)$_{max}$ "seen" by the first pellet	n_e (10^{20} m^{-3}) "seen" by the first pellet
(a) neutral gas shielding				
2000	56.2	61.6	6.0	1.46
4000	67.3	73.0	7.8	1.49
5000	73.0	78.0	8.8	1.51
(b) magnetic shielding approx.				
2000	84.6	96.2	10.9	1.54
4000	119.0	136.5	16.5	1.65
5000	136.5	153.8	18.4	1.69

The temperature and density distributions shown in Fig. 16 corresponds to a D_2 pellet injected with v_p = 5000 m/s and to

neutral gas shielding. The respective curves shown in Fig. 17 correspond to the magnetic shielding approximation. The differences in the respective penetration depths and particle deposition profiles are obvious. Figures 18 and 19 corresponds to the injection of the second (T_2) pellet into the same discharges. As a result of the magnetic shielding assumed, the T_2 pellet practically reaches the plasma center. This can be particularly well seen in Fig. 21, in which the time histories of the central and average electron densities are plotted (compare this figure with Fig. 20, in which the central density is only weakly affected by the injected pellets). The time evolutions of the respective spatial distributions are shown in Figs. 22 and 23. Once more, notable is the central deposition of the ablated T_2 particles when magnetic shielding is assumed.

Part II

The generation of favourable density and temperature profiles in fusion machines by means of pellet injection, or the manipulation of the discharge parameter distributions in general, requires certain minimum penetration depths in fusion plasmas. Full utilization of the possibilities offered by pellet injection in this respect would, in some cases, require central pellet injection, i.e. injective particle transport up to the centre of the plasma column.

In a series of transport calculations we thus investigated pellet size and pellet velocity combinations that would be required for central fuelling of INTOR by using either the standard neutral shielding model for determining the ablation rate or the magnetic shielding approximation defined in Sec. b of Part I of this report.

The results of some representative runs are summarized in Table 2. Two pellets were injected into the ignited reference plasma (see p. 3/4) at t = 9 s (D_2 pellet) and t = 10 s (T_2 pellet). The penetration depths of the two pellets are displayed in Table 2 for various pellet sizes and injection velocities for both the neutral shielding model and the magnetic shielding approximation (plasma radius in INTOR: a = 162.4 cm). Note that penetration depth is defined as the innermost plasma radius affected by injected pellet particles. The bulk of the pellet mass is deposited outside this radius.

Table 2: Data on pellet sizes and injection velocities required for central fuelling in INTOR. Plasma radius: a = 162.4 cm.

Pellet radius (cm)	Pellet velocity (10^3 m/s)	Penetration depths (cm) D_2 pellet	T_2 pellet
Neutral gas shielding model			
0.3	10.	73.	73.
0.3	18.	87.	90.
0.5	14.	125.	162.
0.5	16.	131.	171.
0.525	10.	119.	148.
0.6	10.	142.	325.
0.7	10.	206.	325.
Magnetic shielding approximation			
0.3	3.	90.	96.
0.3	5.	113.	125.
0.3	6.	125.	142.
0.3	7.	137.	154.
0.3	8.	148.	165.
0.4	5.	160.	177.
0.4	6.	182.	194.
0.4	7.	200.	217.
0.525	3.	171.	200.

The following conclusions may be drawn from the computed data:

(a) If the neutral gas shielding model also holds under reactor plasma conditions, pellets of sufficiently small size, i.e. those not causing more than 10 % $\langle n \rangle$ perturbation, could not be used for central fuelling because of the extreme velocity requirements ($v_p = 1.8 \times 10^4$ m/s applied to $r_p = 0.3$ cm only yields penetration depths of 86 to 90 cm). Even if pellet sizes corresponding to $\langle n \rangle$ increases of over 100 % were found

acceptable for some special purposes (density ramp-up, etc.) pellet velocities of over 10^4 m/s would be necessary for central particle deposition.

(b) If the anticipated magnetic shielding is of the same order of magnitude as assumed in Sec. b of Part I, central fuelling with 10 % perturbation of the average plasma density in INTOR would require an injection velocity of 9200 m/s (or 5200 m/s for $r_p \approx 0.4$ cm and 3000 m/s for $r_p \approx 0.5$ cm).

(c) The present injection technology yields pellet velocities of under 2000 m/s. No injection method is envisaged at present for pellet velocities of over 10^4 m/s, not even for single pellets (the technical requirements associated with continuous fuelling always being more difficult). Injection velocities of several 10^3 m/s, probably up to 5000 m/s, are conceivable, but the associated technological difficulties are rather severe.

(d) If the pellet shielding in reactor plasmas is not larger than that predicted by neutral shielding theory, the application of pellets to reactor plasmas will be limited to edge fuelling.

(e) To assess the true potentials of pellet injection in reactor plasmas, accurate estimates of the pellet ablation rate under thermonuclear plasma conditions are urgently needed. The development of comprehensive ablation models appears to be an important task even for the next generation of fusion machines.

References

/1/ C.T.Chang, L.W.Jørgensen, P.Nielsen, and L.L.Lengyel, Nucl. Fus. 20 (1980), 859.

/2/ G.L.Schmidt, PPPL, private communication (1983).

/3/ M.Greenwald et al., Phys. Rev. Lett. 53 (1984), 352; see also MIT Pl. Fus. Center Repts. PFC/CP-83-10 (Sept. 1983) and PFC/CP-84-2 (May 1984).

/4/ L.L.Lengyel, NET Internal Note 83-102 (Aug. 1093).

/5/ L.L.Lengyel, IPP 1/213, March 1983.

/6/ P.B.Parks, R.S.Turnbull, and C.A.Foster, Nucl. Fus. 17 (1977), 539; see also S.C.Milora and C.A.Foster, IEEE Trans. Pl. Sci. 6 (1978), 578.

/7/ D.E.Post, C.E.Singer, A.M.McKenney, et al., PPPL Rept. 33 (1981).

/8/ L.L.Lengyel, Phys. Fluids 21 (1978), 1945.

/9/ P.C.Souers, LLL Rept. UCRL-52226 (1977).

/10/ C.E.Thomas, ORNL/TM-7486, Oak Ridge (1981).

/11/ M.Kaufmann, K.Lackner, L.Lengyel, and W.Schneider, Verhandl. DPG (VI) 19 (1984), 1210.

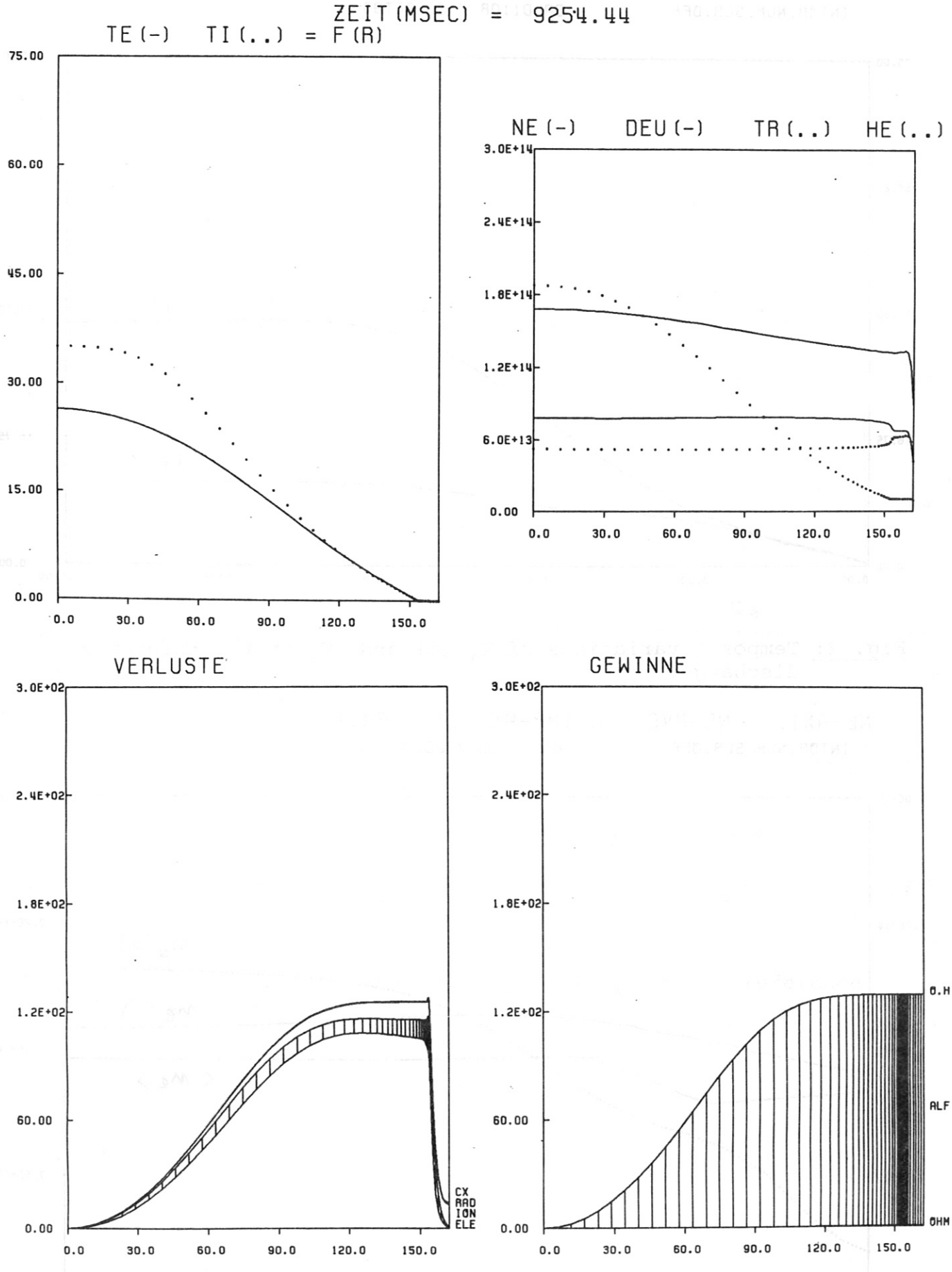

Fig. 1: Radial distributions of plasma parameters and energy gains and losses in the reference discharge.

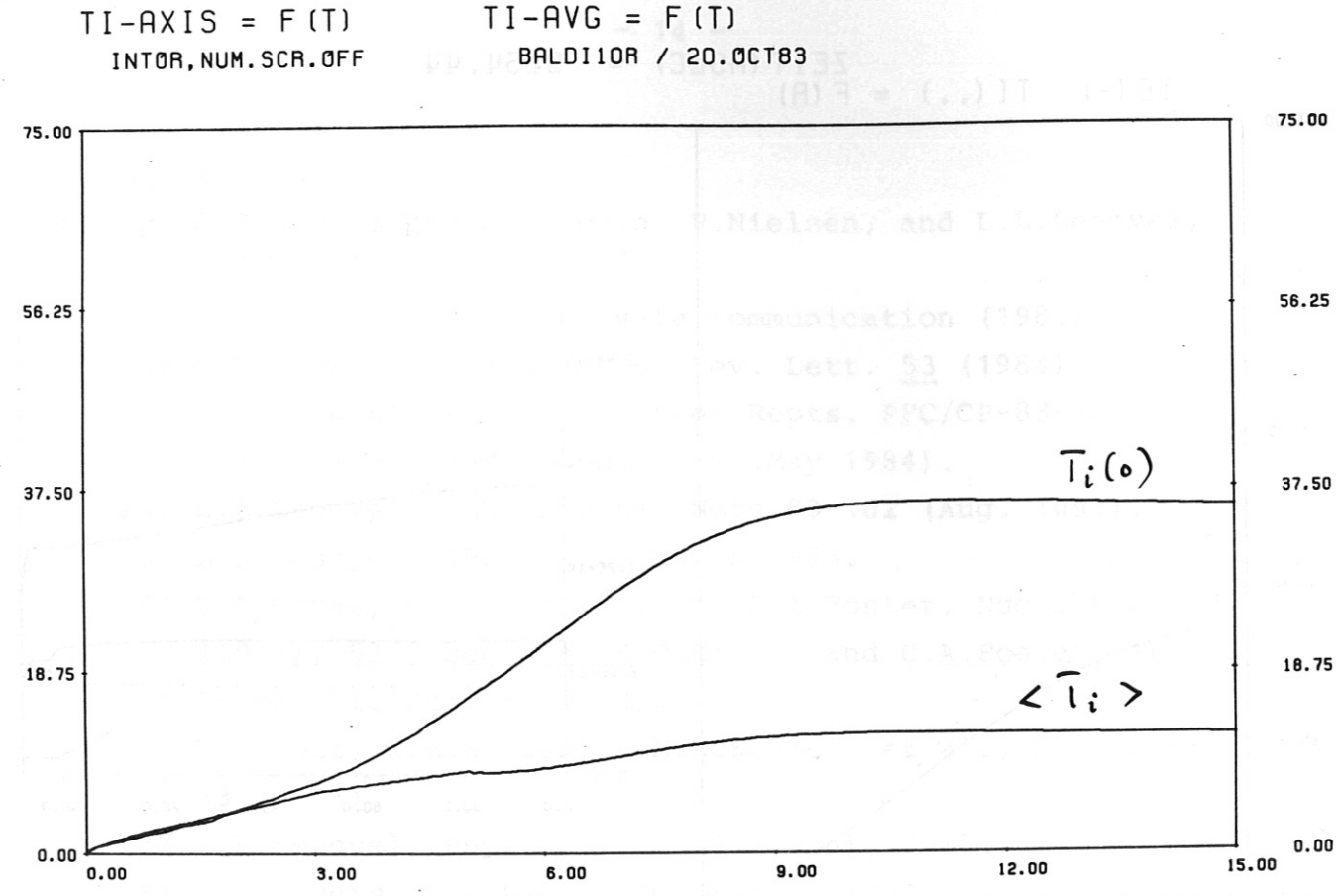

Fig. 2: Temporal variations of T_i (o) and T_i in the reference discharge.

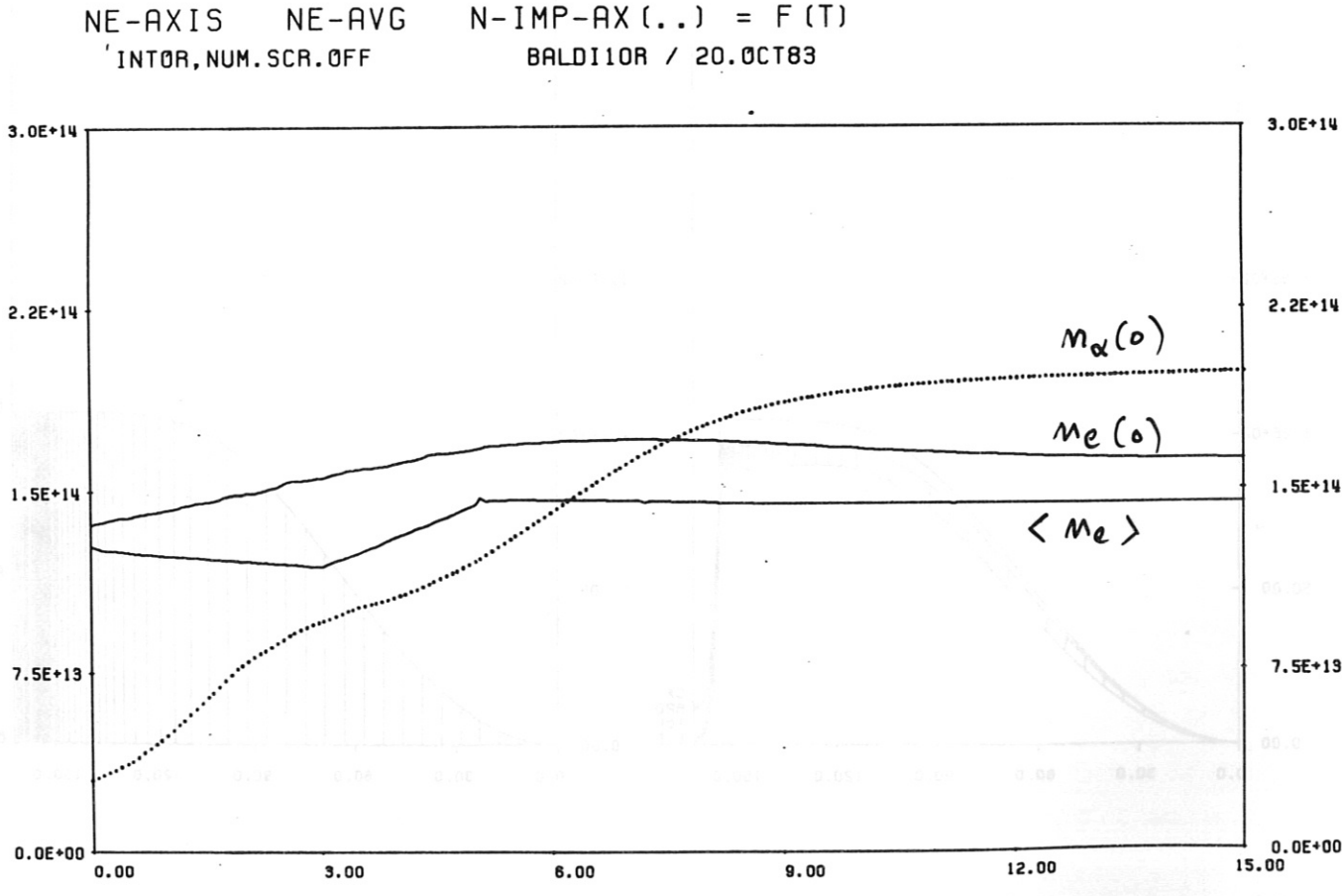

Fig. 3: Temporal variations of $n_e(o)$, $\langle n_e \rangle$, and $n_\alpha(o)$ in the reference discharge.

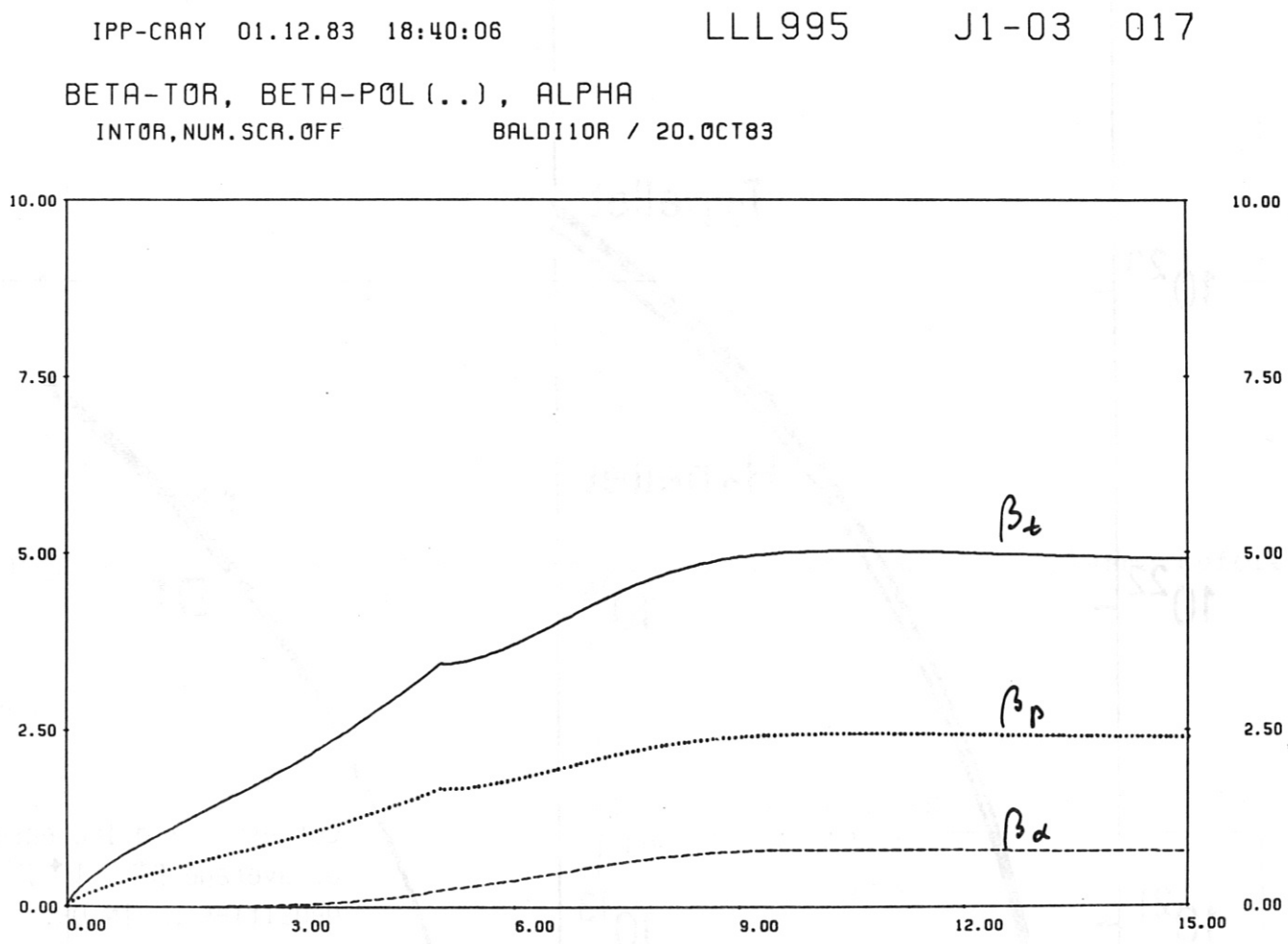

Fig. 4: Temporal variations of β_t, β_p, and β_α in the reference discharge.

Fig. 5

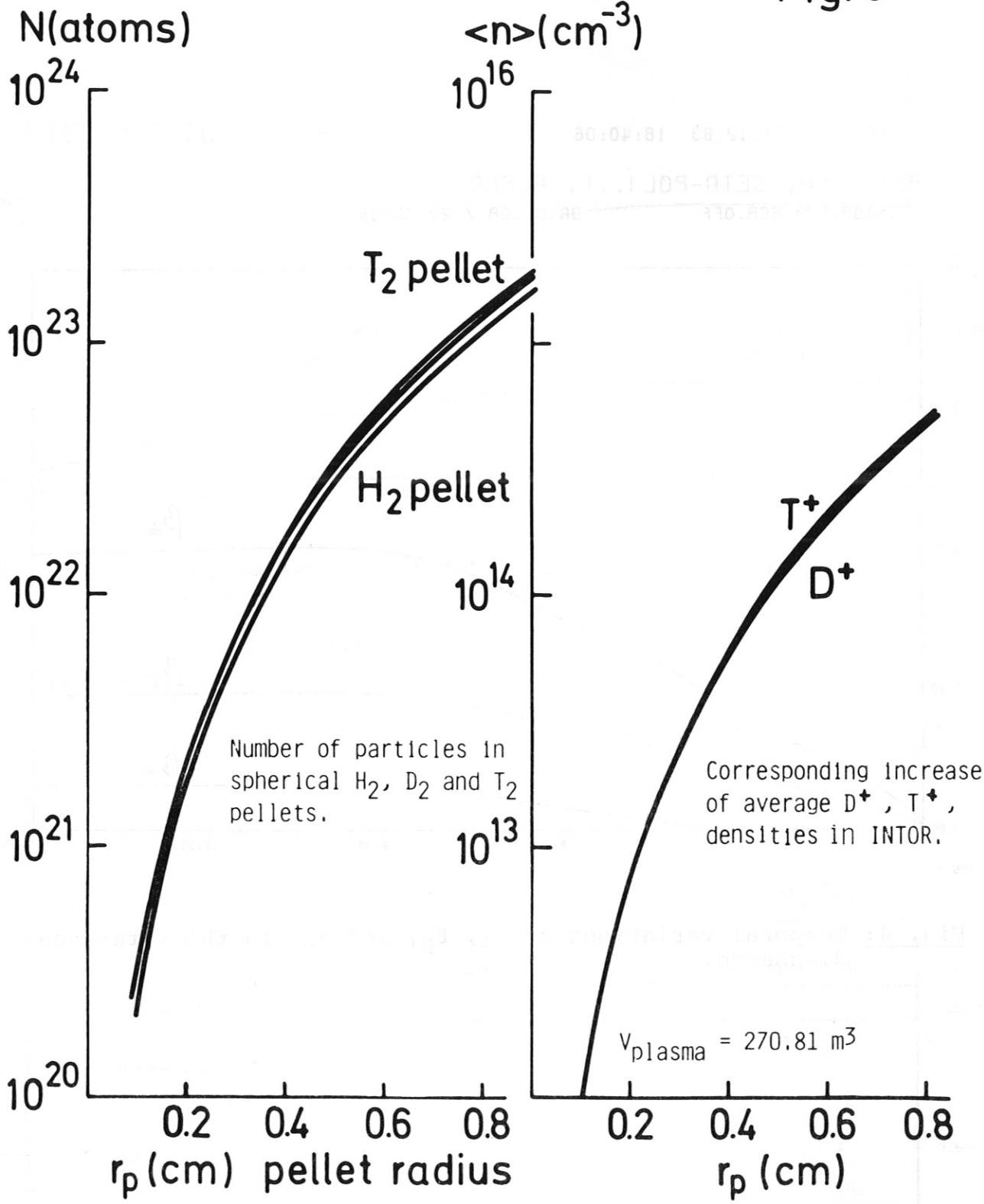
N(atoms)
10^{24}
10^{23}
10^{22}
10^{21}
10^{20}
T_2 pellet
H_2 pellet
Number of particles in spherical H_2, D_2 and T_2 pellets.
0.2
0.4
0.6
0.8
r_p (cm) pellet radius
<n>(cm^{-3})
10^{16}
10^{14}
10^{13}
T^+
D^+
Corresponding increase of average D^+, T^+, densities in INTOR.
V_{plasma} = 270.81 m^3
0.2
0.4
0.6
0.8
r_p (cm)

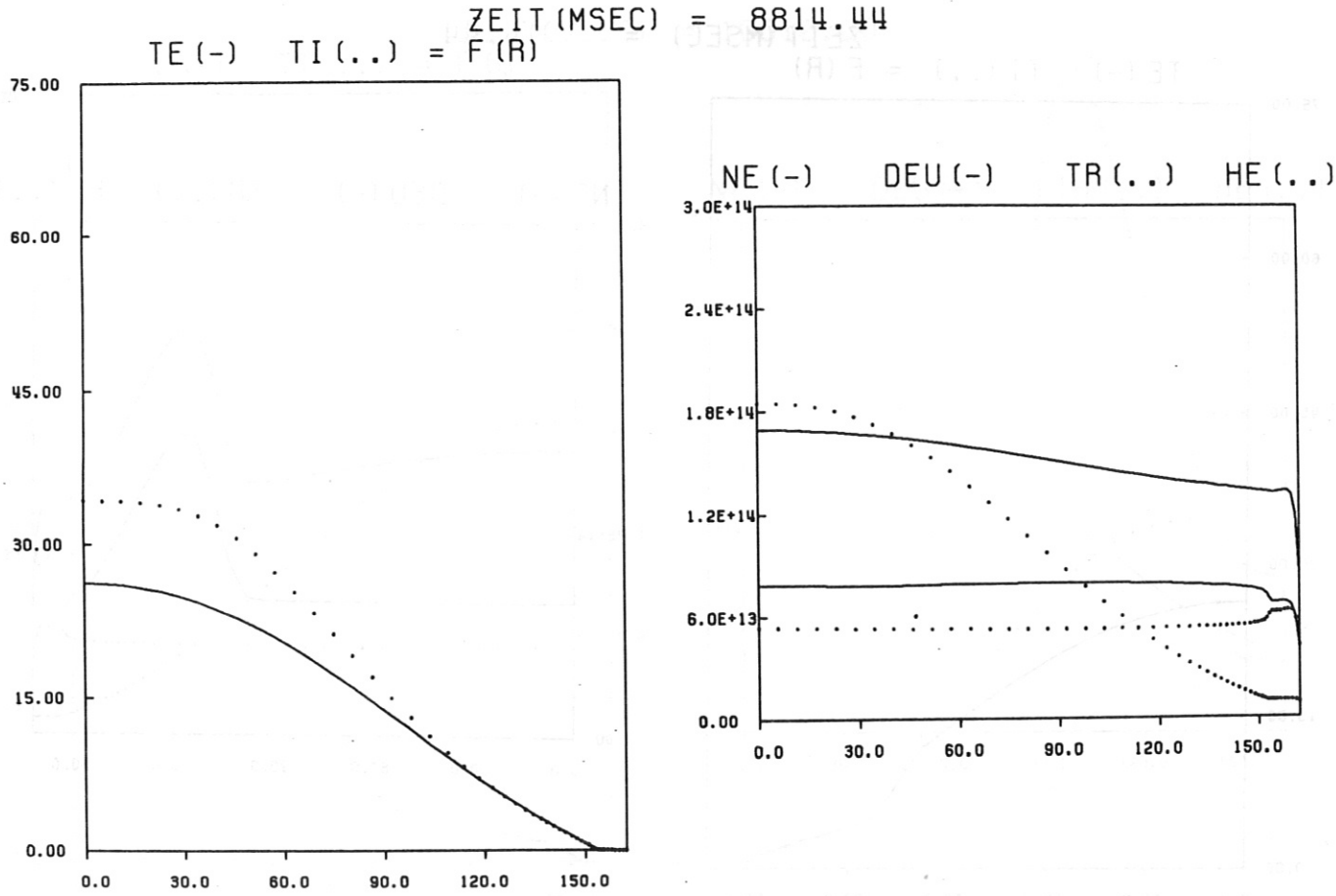

Fig. 6: Plasma parameter distributions in the recipient plasma before pellet injection.

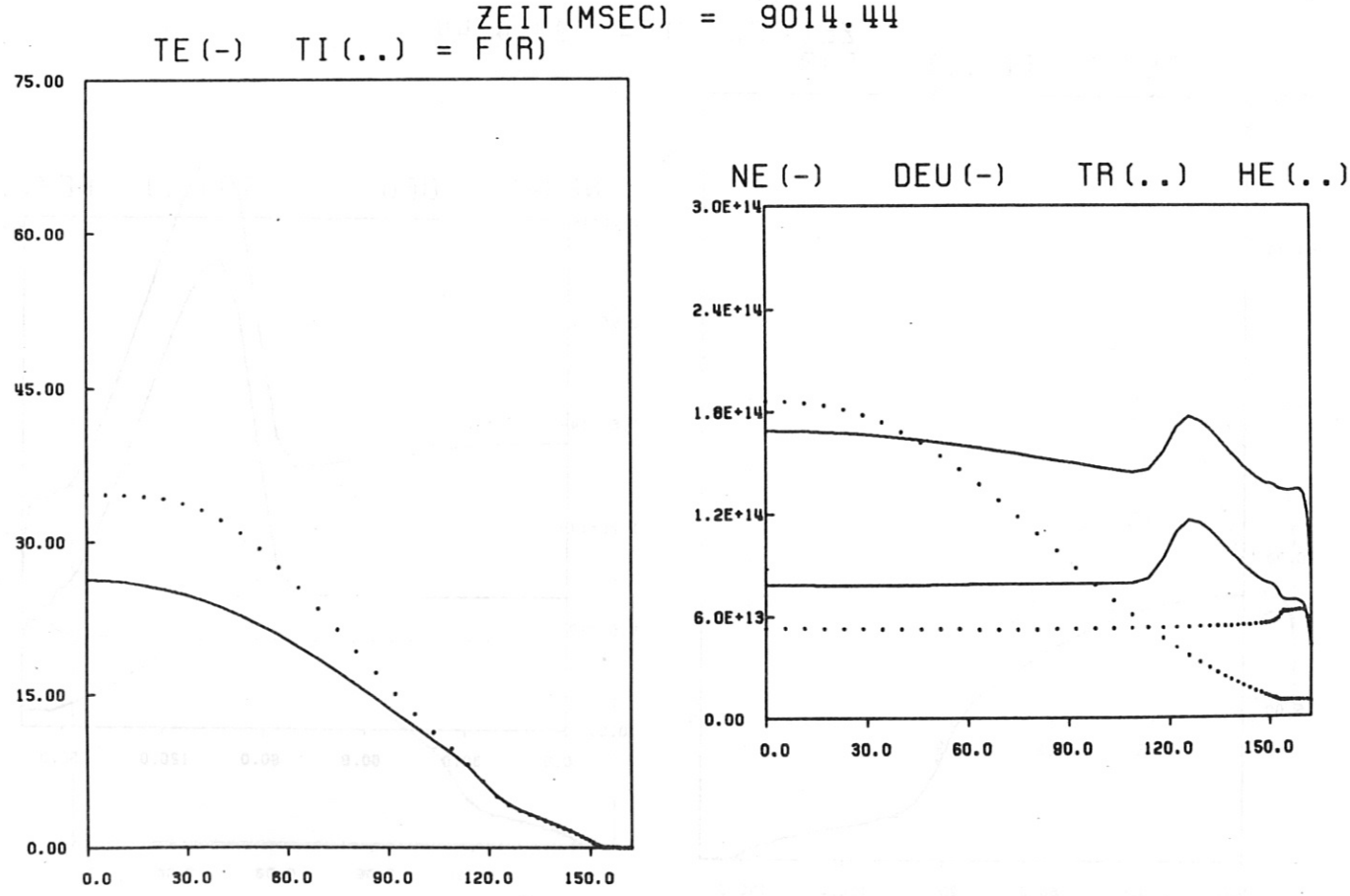

Fig. 7: 1st (D_2) pellet injected, v_p = 4000 m/s, r_p = 0.2 cm, neutral gas shielding ablation model.

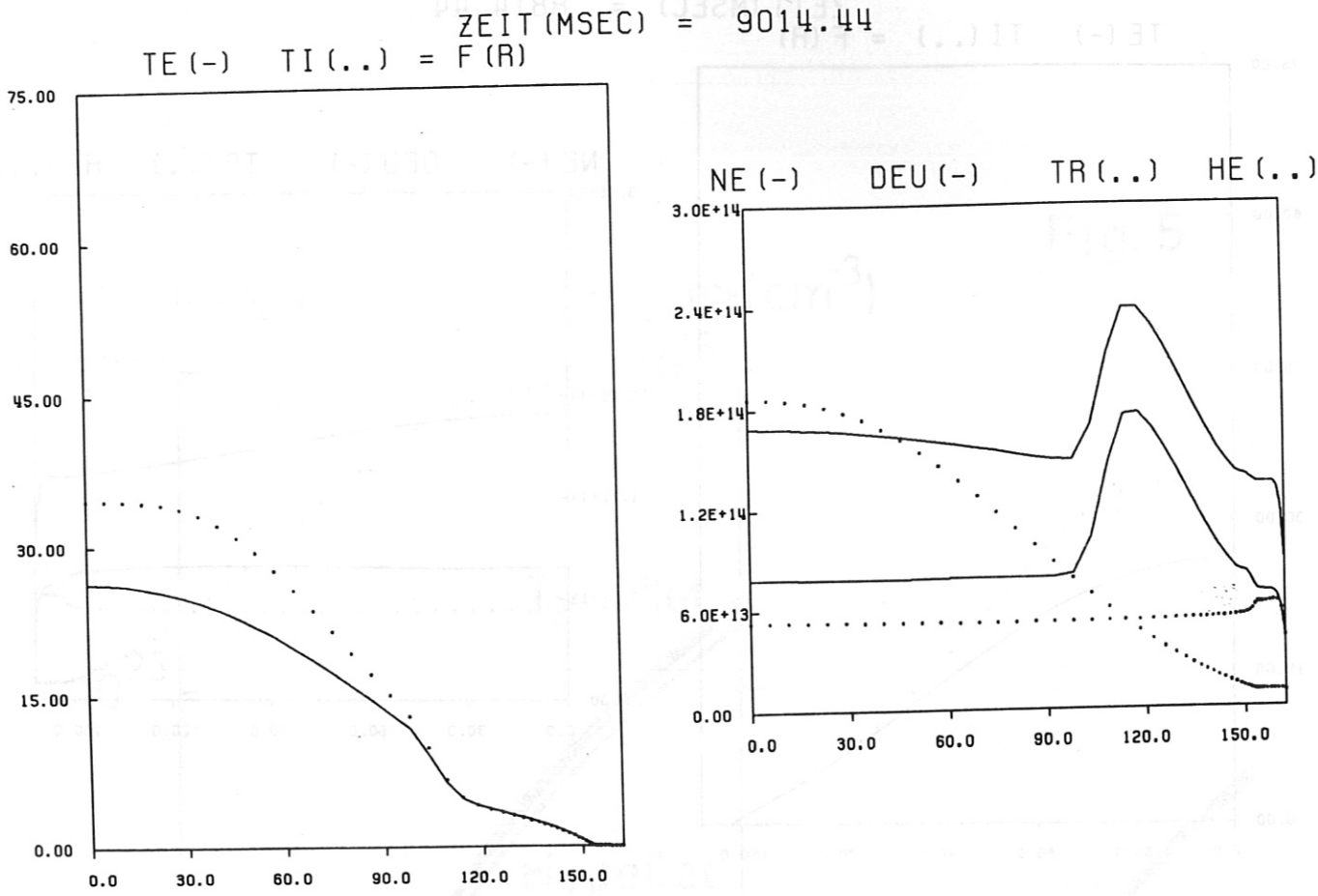

Fig. 8: 1st (D_2) pellet injected, v_p = 4000 m/s, r_p = 0.3 cm, neutral gas shielding ablation model.

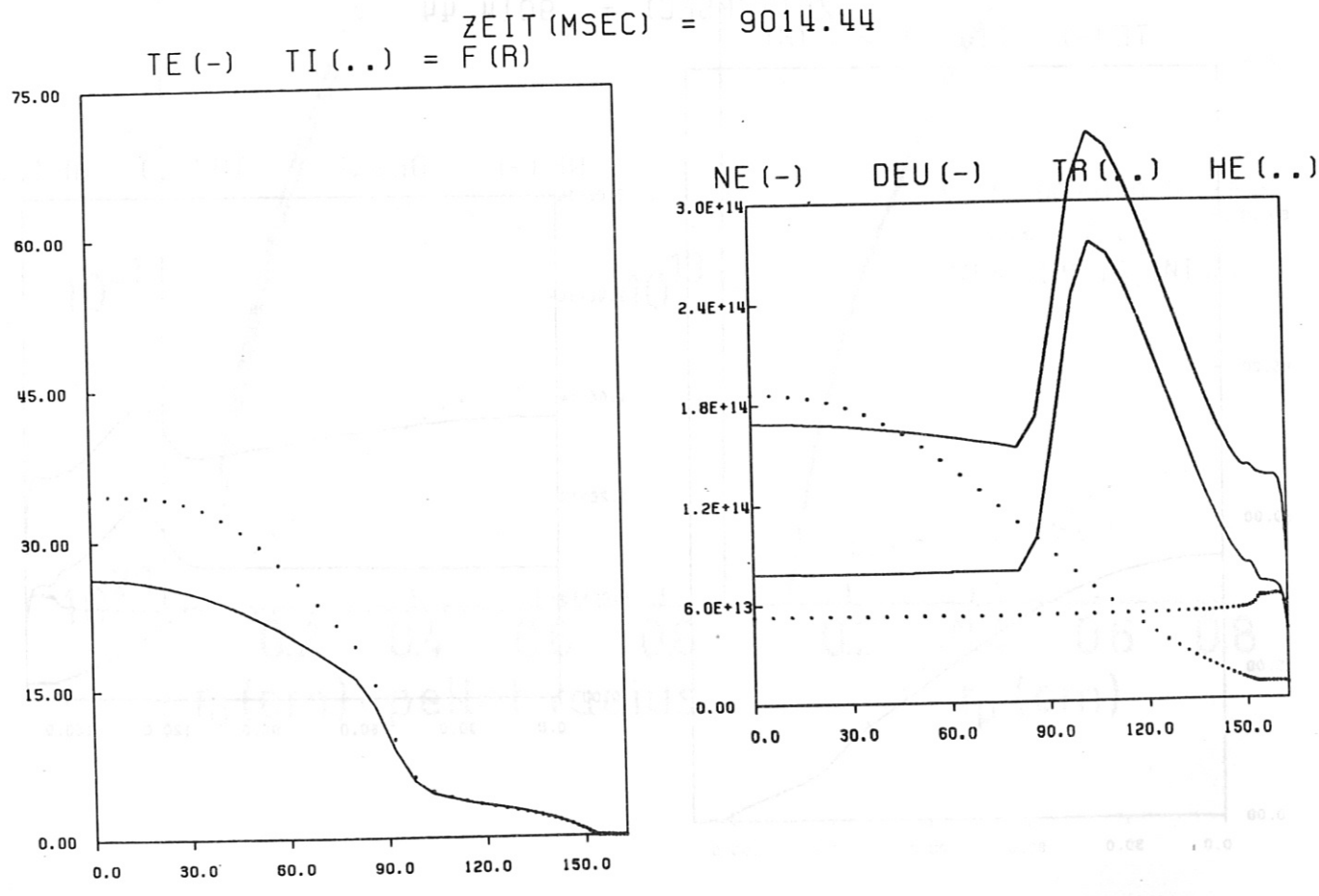

Fig. 9: 1st (D_2) pellet injected, v_p = 4000 m/s, r_p = 0.4 cm, neutral gas shielding ablation model.

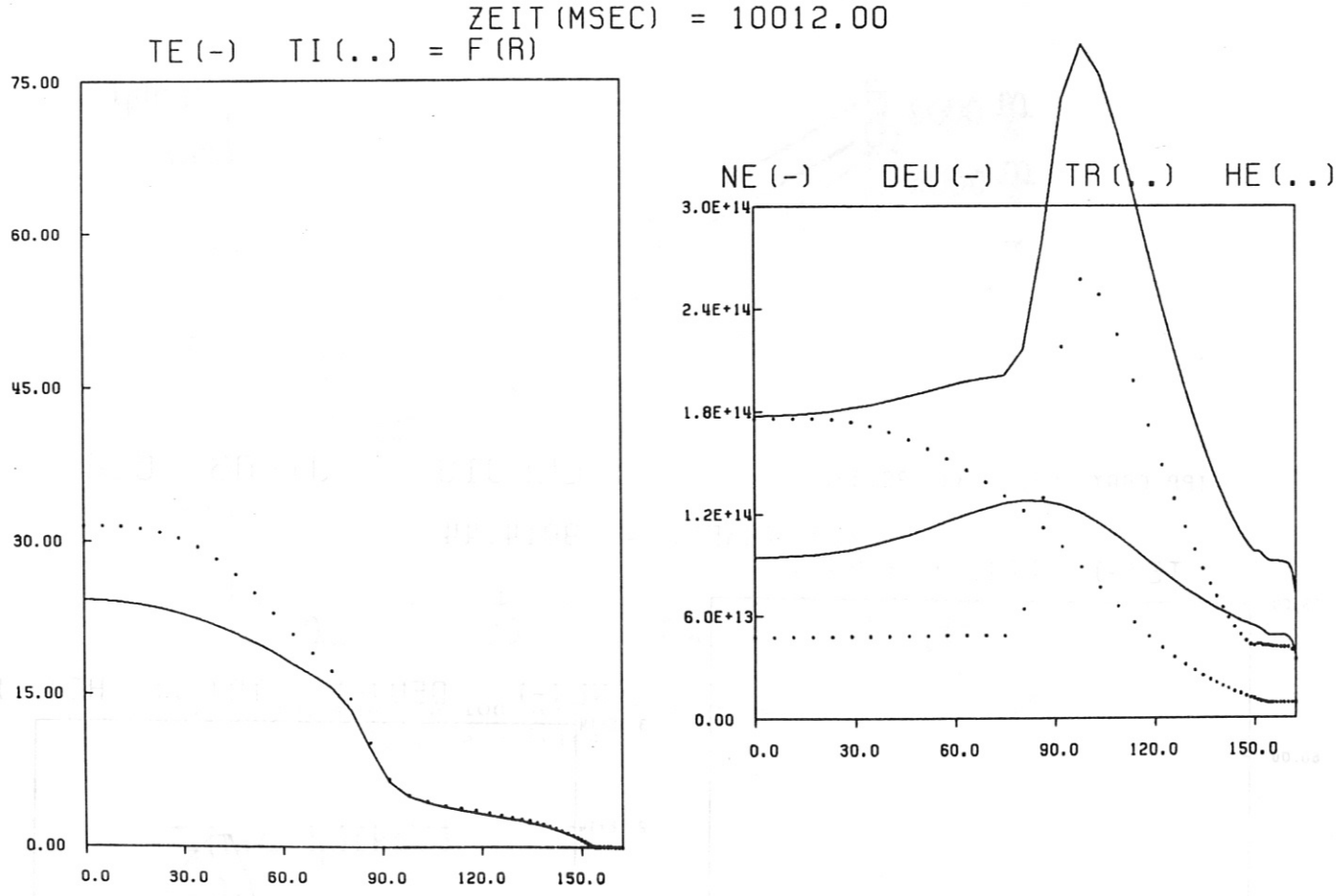

Fig. 10: 2nd (T_2) pellet injected, v_p = 4000 m/s, r_p = 0.4 cm, neutral gas shielding ablation model.

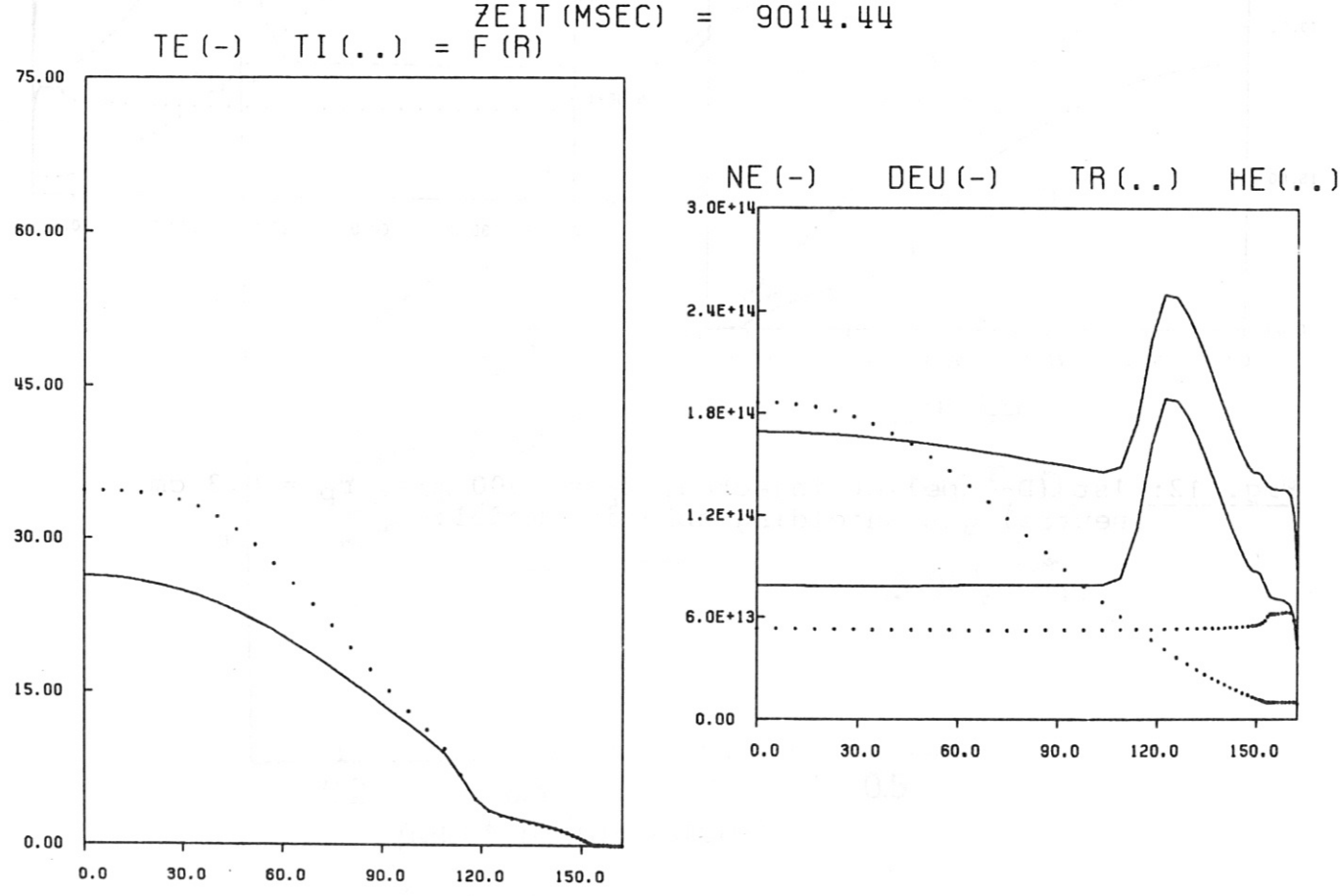

Fig. 11: 1st (D_2) pellet injected, v_p = 2000 m/s, r_p = 0.3 cm, neutral gas shielding ablation model.

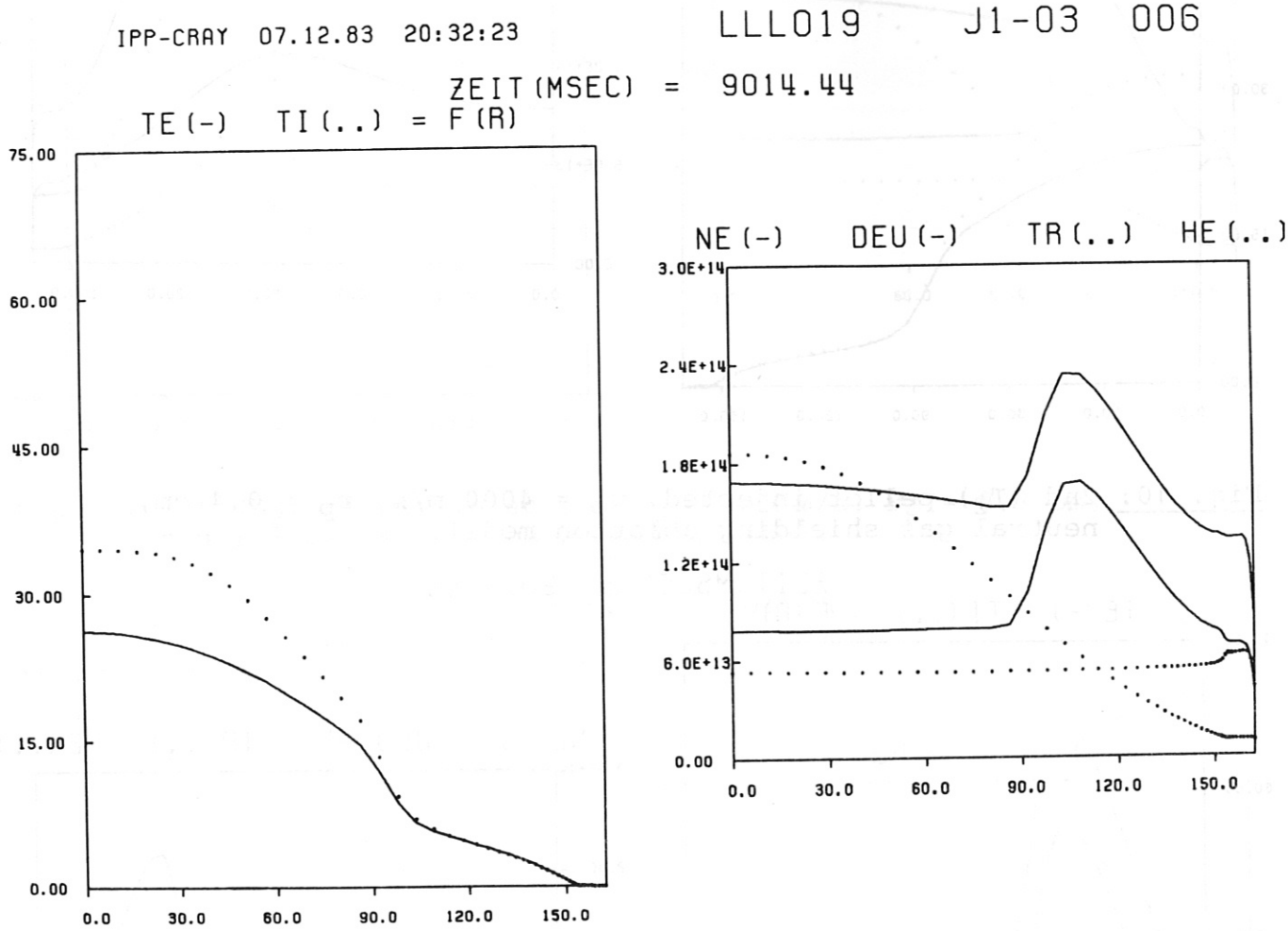

Fig. 12: 1st (D_2) pellet injected, v_p = 8000 m/s, r_p = 0.3 cm, neutral gas shielding ablation model.

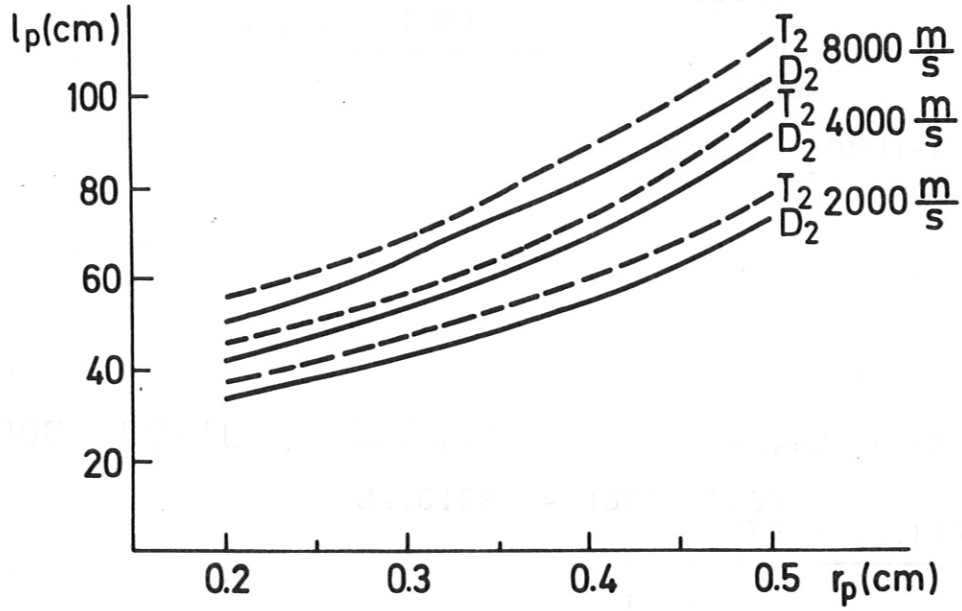

Fig. 13: Penetration depths vs. pellet radius for different pellet velocities.

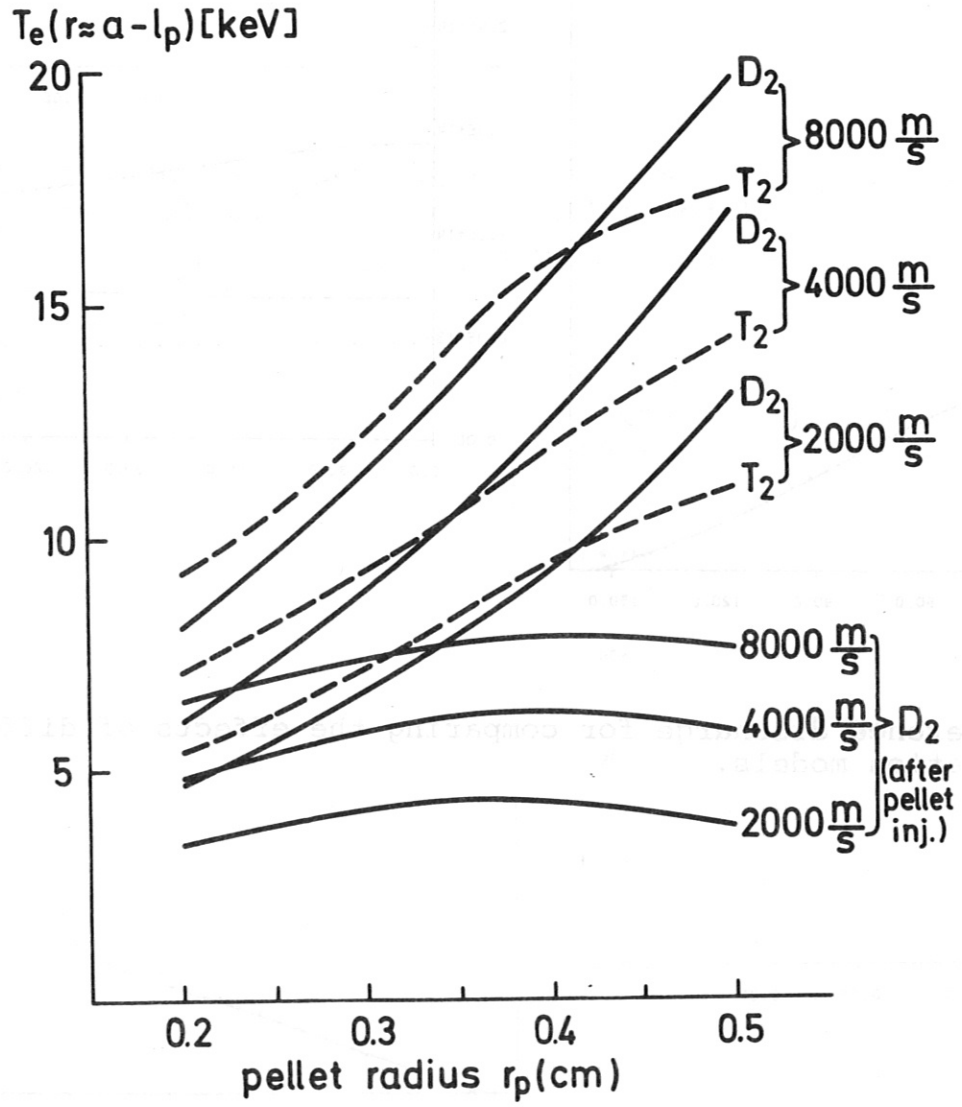

Fig. 14: Maximum temperatures "seen" by pellets at maximum penetration depths and temperatures after adiabatic cooling.

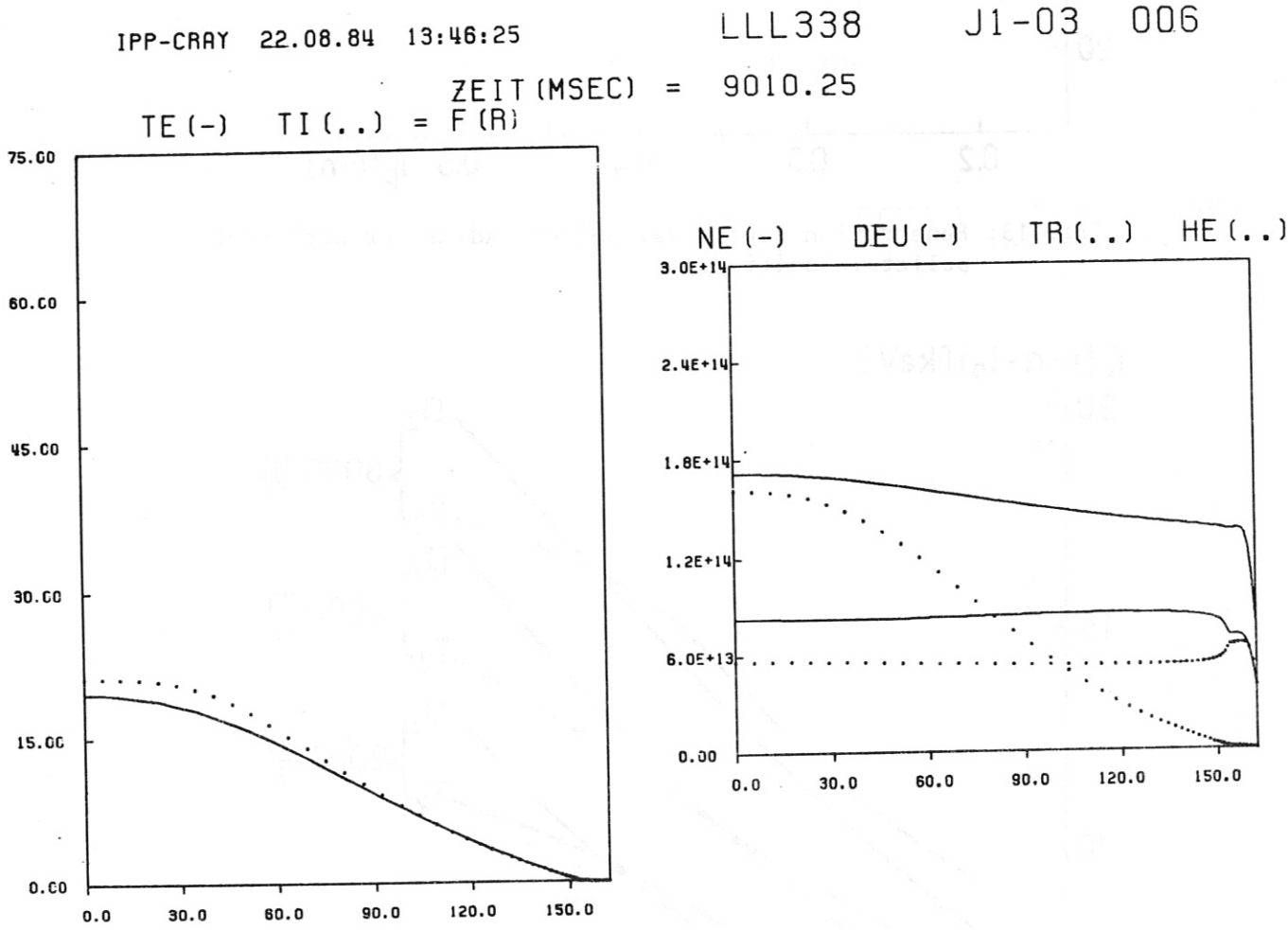

Fig. 15: Reference discharge for comparing the effects of different ablation models.

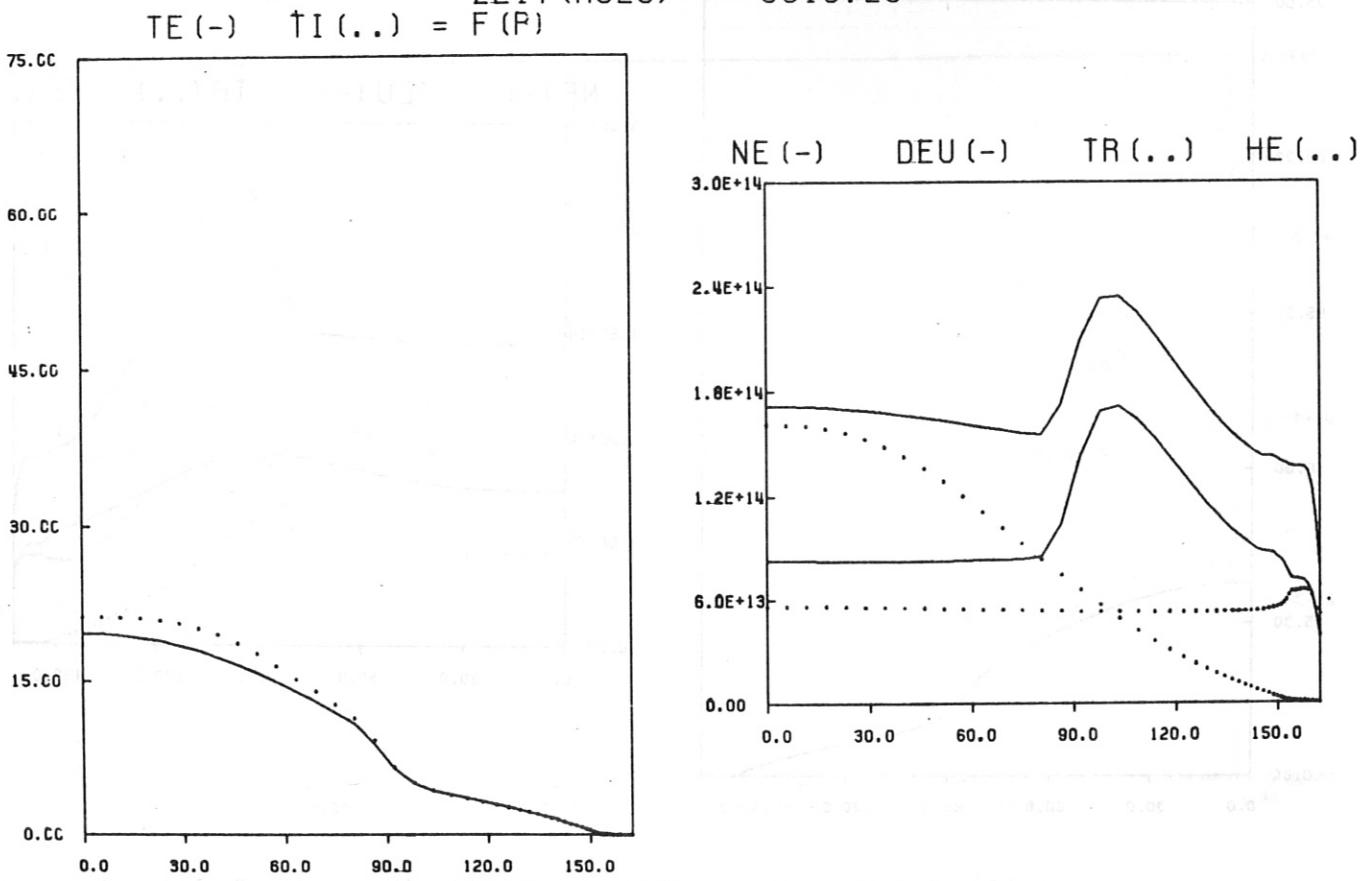

Fig. 16: 1st (D_2) pellet injected, v_p = 5000 m/s, r_p = 0.3 cm, neutral gas shielding ablation model.

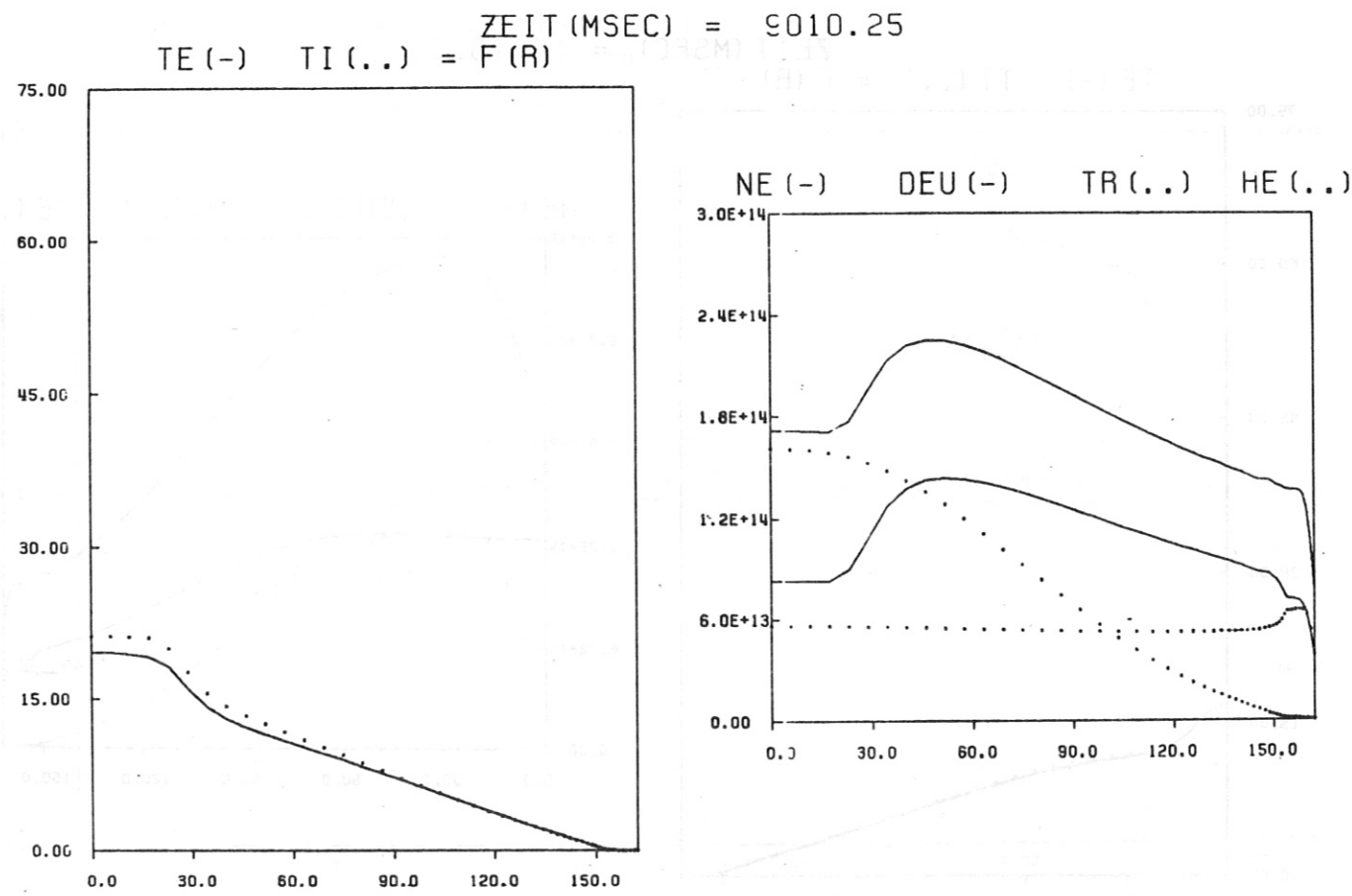

Fig. 17: 1st (D_2) pellet injected, v_p = 5000 m/s, r_p = 0.3 cm, magnetic shielding approximation.

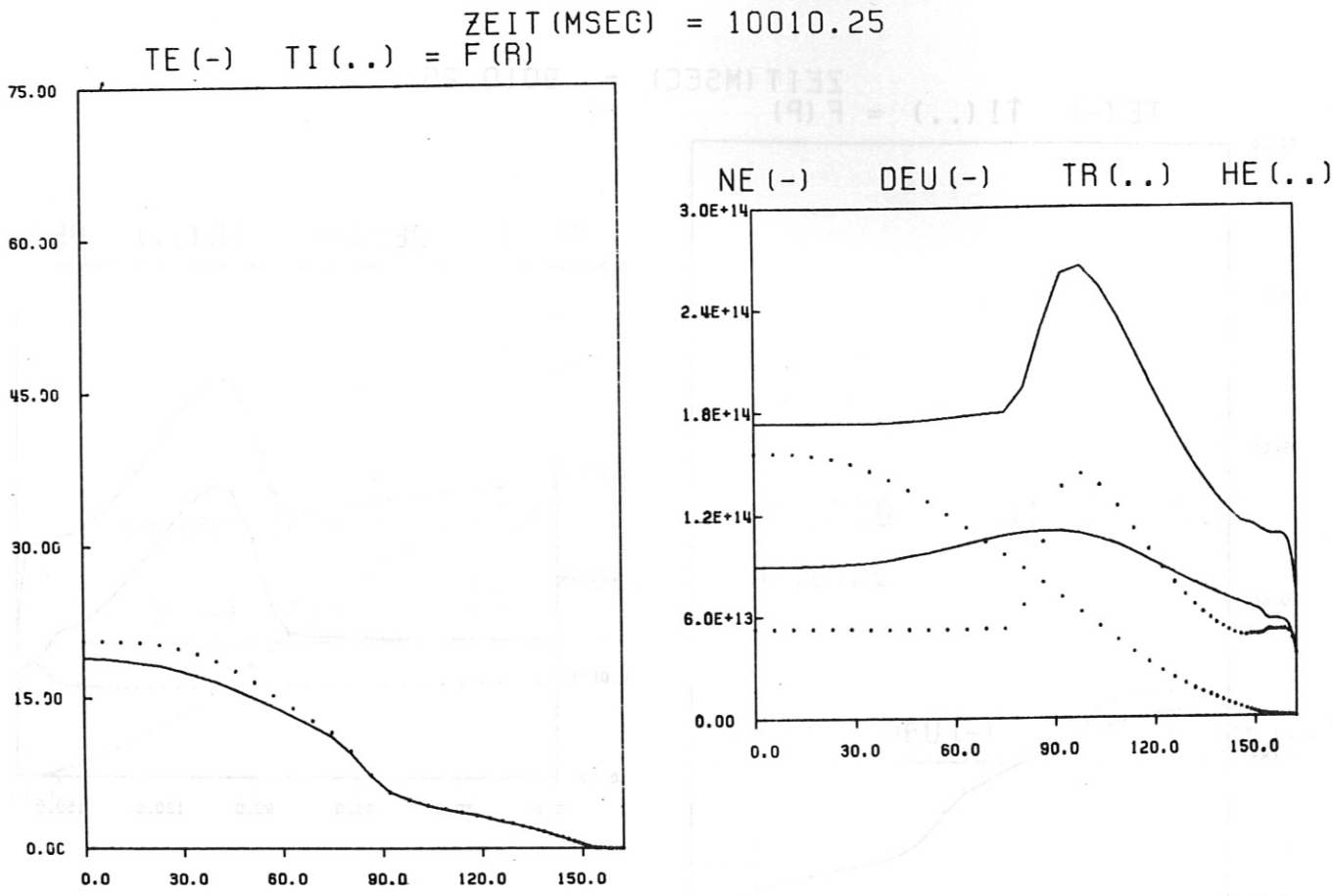

Fig. 18: 2nd (T_2) pellet injected, v_p = 5000 m/s, r_p = 0.3 cm, neutral gas shielding model.

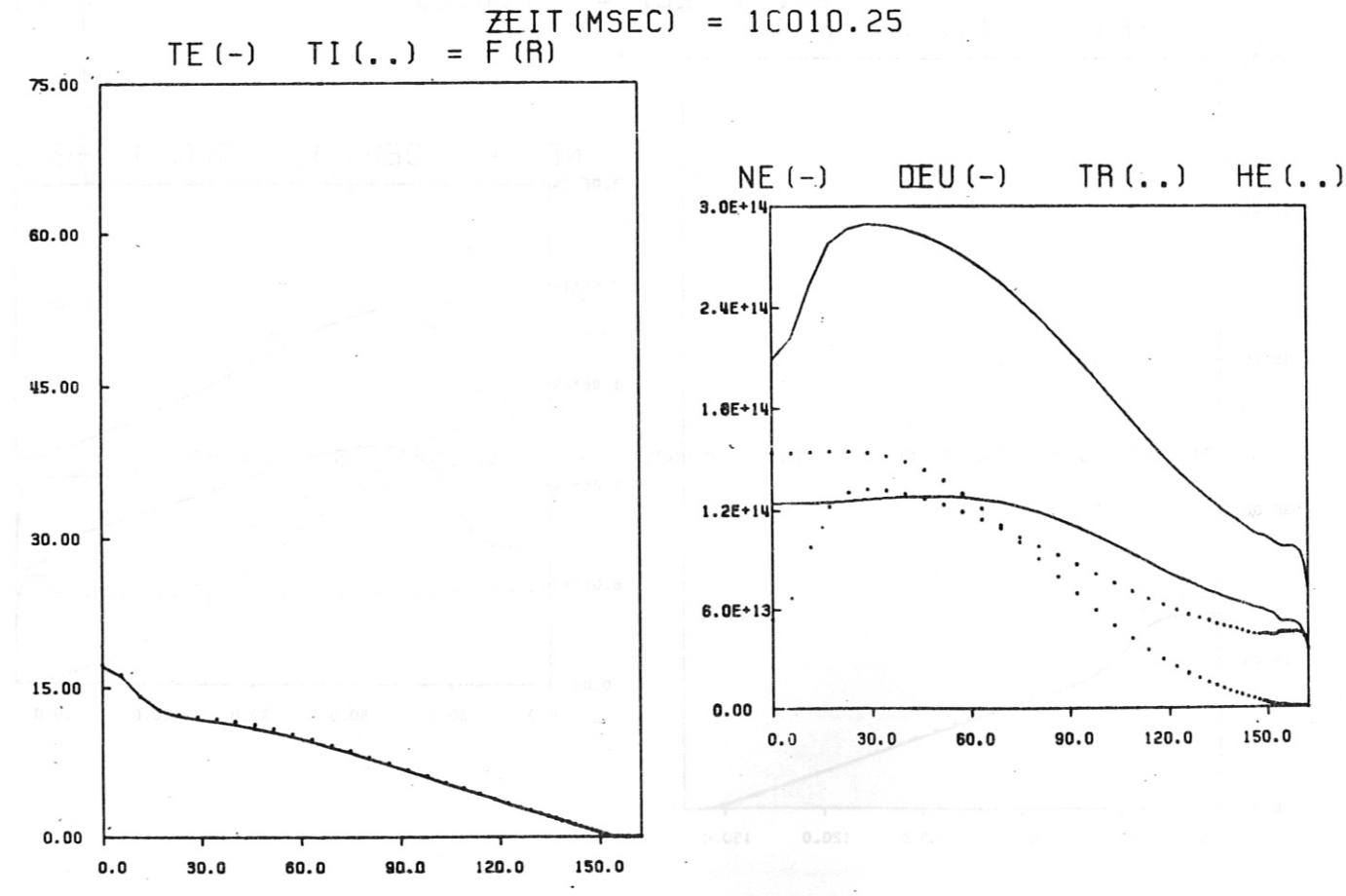

Fig. 19: 2nd (T_2) pellet injected, v_p = 5000 m/s, r_p = 0.3 cm, magnetic shielding approximation.

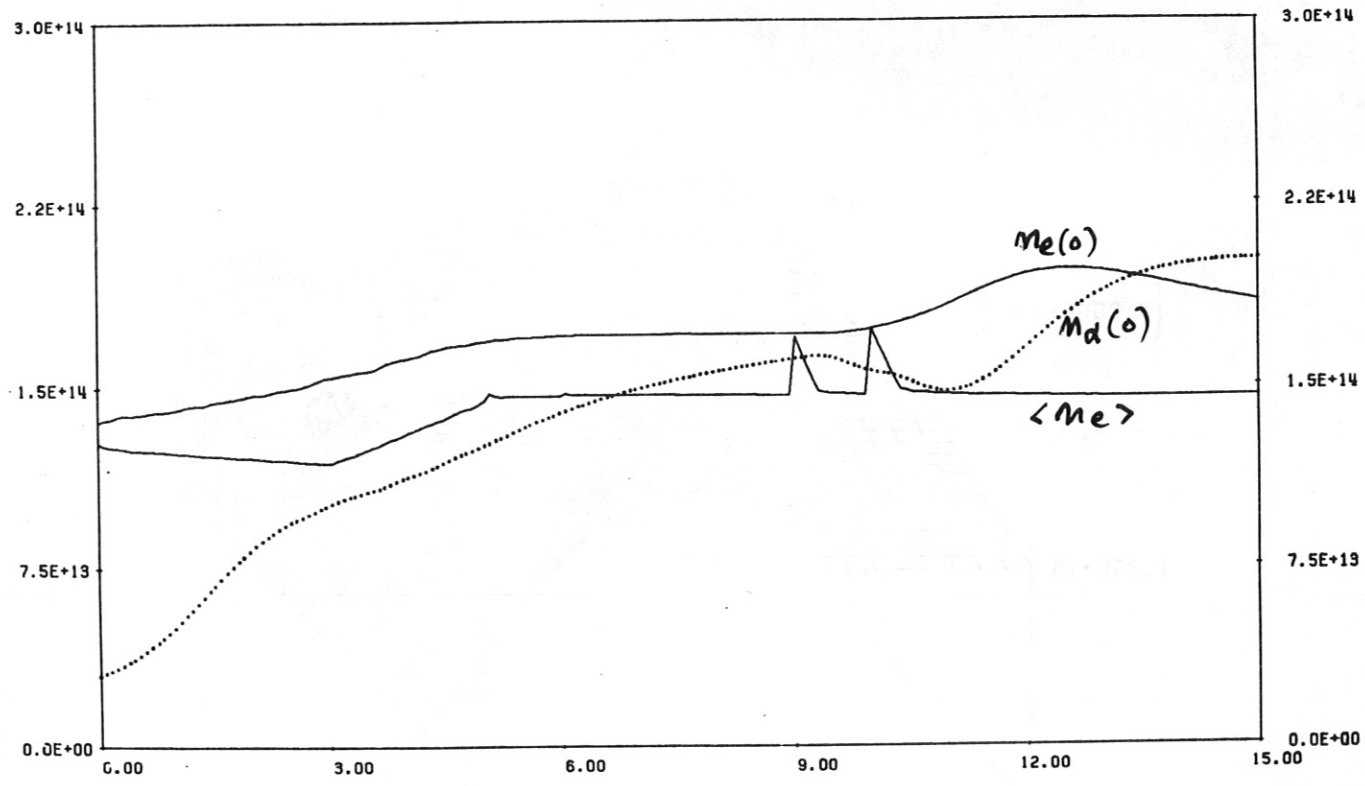

Fig. 20: Temporal variation of $n_e(o)$, $\langle n_e \rangle$, and $n_\alpha(o)$, v_p = 5000 m/s, r_p = 0.3 cm, neutral gas shielding ablation model.

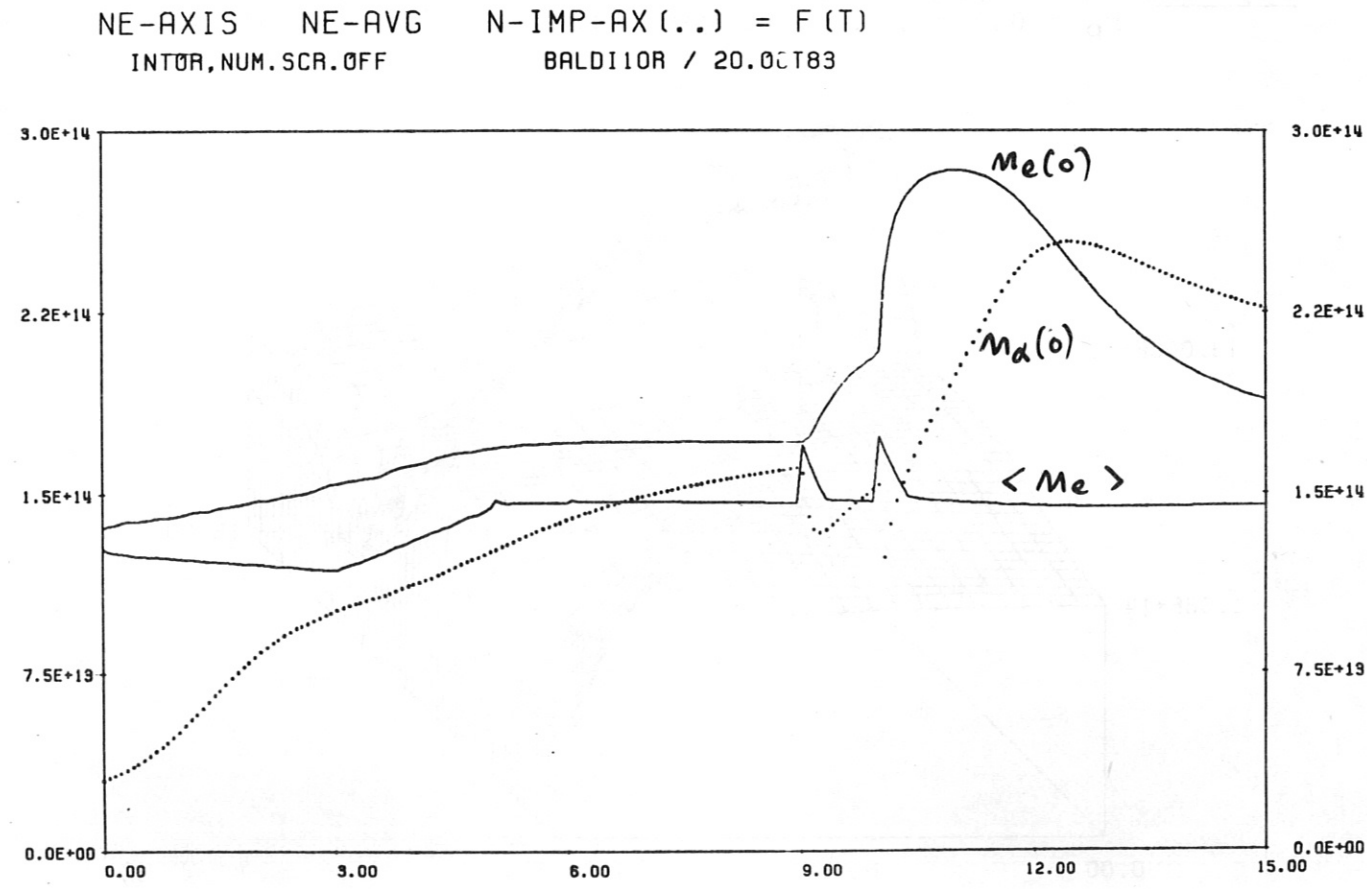

Fig. 21: Temporal variation of $n_e(o)$, $\langle n_e \rangle$, and $n_\alpha(o)$, v_p = 5000 m/s, r_p = 0.3 cm, magnetic shielding approximation.

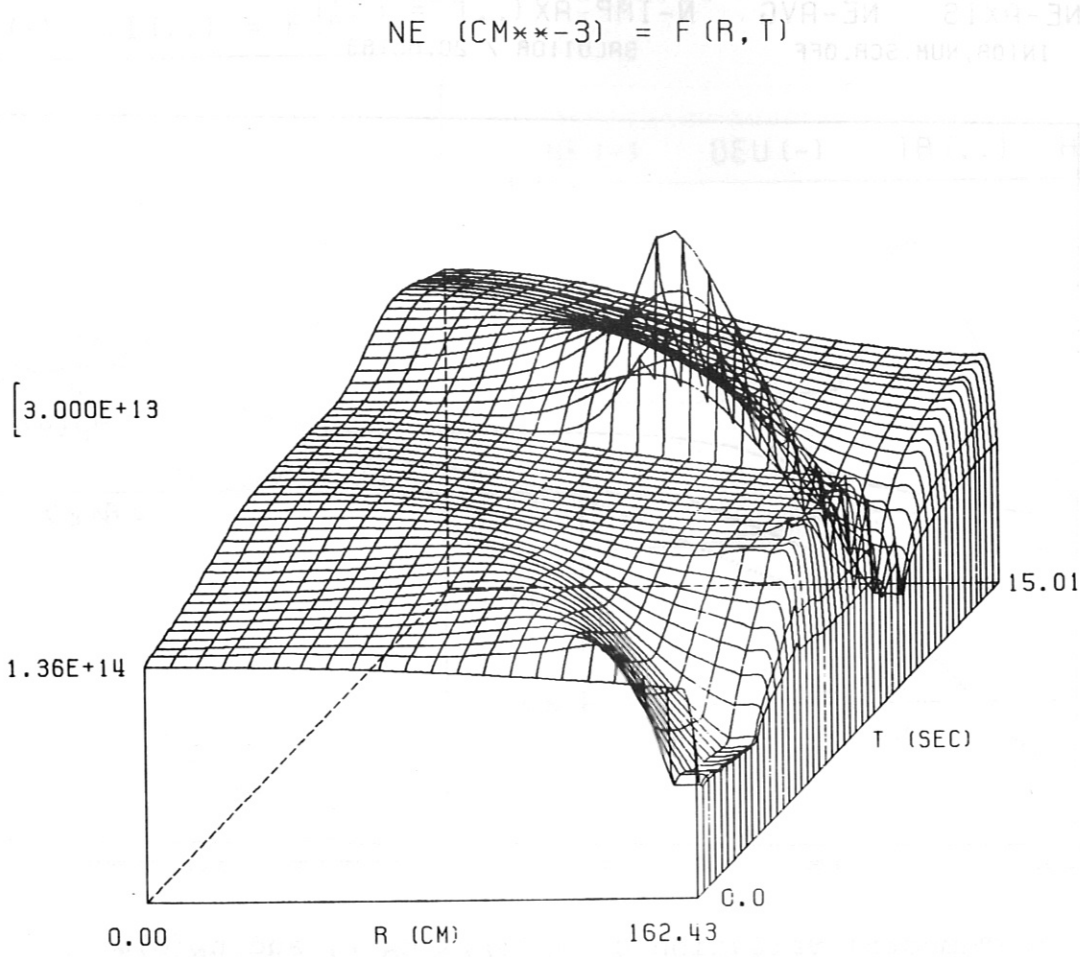

Fig. 22: Time evolution of the $n_e(r)$ distribution, v_p = 5000 m/s, r_p = 0.3 cm, neutral gas shielding ablation model.

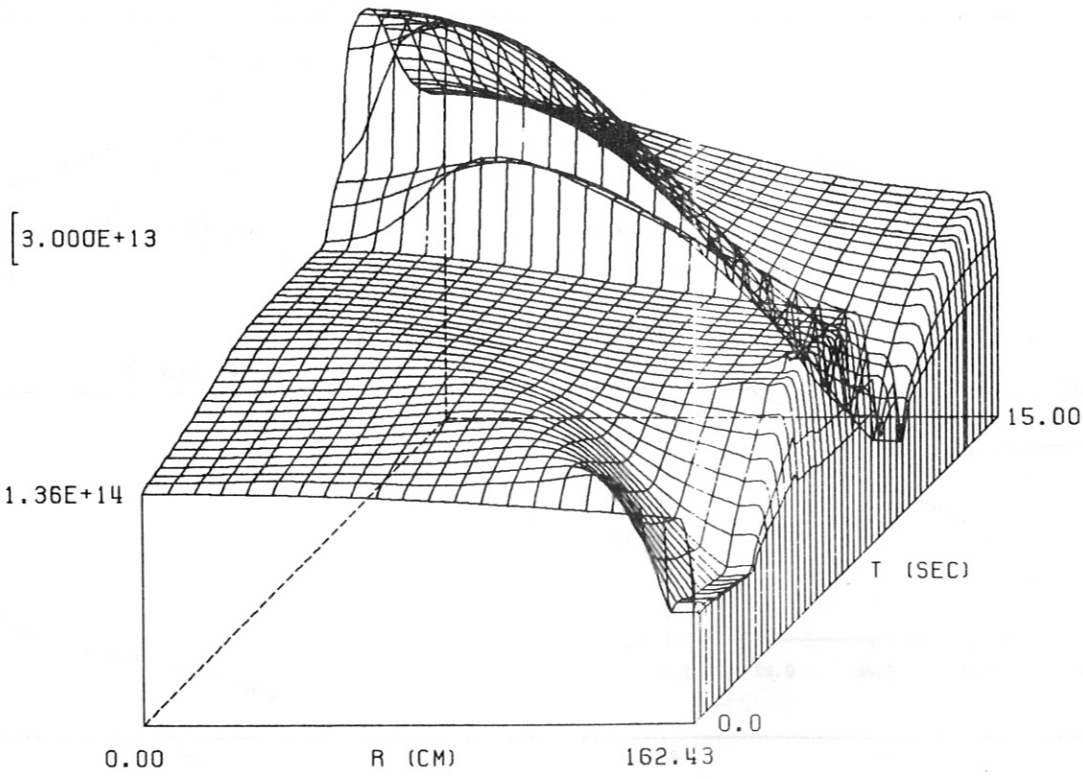

Fig. 23: Time evolution of the $n_e(r)$ distribution, v_p = 5000 m/s, r_p = 0.3 cm, magnetic shielding approximation.